





# Cosmological Evolution of the Formation Rate of Short Gamma-Ray Bursts with and without Extended Emission

M. G. Dainotti<sup>1,2,7</sup> , V. Petrosian<sup>3,4,5</sup> , and L. Bowden<sup>6</sup>

<sup>1</sup> National Astronomical Observatory of Japan, Mitaka, Tokyo, Japan; [maria.dainotti@nao.ac.edu.jp](mailto:maria.dainotti@nao.ac.edu.jp)

<sup>2</sup> Space Science Institute, Boulder, CO, USA

<sup>3</sup> Department of Physics, Stanford University, Via Pueblo Mall 382, Stanford, CA 94305-4060, USA; [vahep@stanford.edu](mailto:vahep@stanford.edu)

<sup>4</sup> Kavli Institute of Particle Astrophysics and Cosmology, Stanford University, Stanford, CA, USA

<sup>5</sup> Department of Applied Physics, Stanford University, Stanford, CA, USA

<sup>6</sup> Cornell University, Ithaca, NY, USA

<sup>7</sup> The Graduate University for Advanced Studies, Shonan Village, Hayama, Kanagawa 240-0193, Japan

Received 2020 October 4; revised 2021 March 26; accepted 2021 April 6; published 2021 June 24

## Abstract

Originating from neutron star–neutron star or neutron star–black hole mergers, short gamma-ray bursts (SGRBs) are the first electromagnetic emitters associated with gravitational waves (GWs). This association makes the determination of SGRB formation rate (FR) a critical issue. We determine the true SGRB FR and its relation to the cosmic star formation rate (SFR). This can help in determining the expected GW rate involving small mass mergers. We present nonparametric methods for the determination of the evolutions of the luminosity function (LF) and the FR using SGRBs observed by Swift, without any assumptions. These are powerful tools for small samples, such as our sample of 68 SGRBs. We combine SGRBs with and without extended emission (SEE), assuming that both descend from the same progenitor. To overcome the incompleteness introduced by redshift measurements we use the Kolmogorov–Smirnov (KS) test to find flux thresholds yielding a sample of sources with a redshift drawn from the parent sample including all sources. Using two subsamples of SGRBs with flux limits of  $4.57 \times 10^{-7}$  and  $2.15 \times 10^{-7}$  erg cm<sup>-2</sup> s<sup>-1</sup> with respective KS  $p = (1, 0.9)$ , we find a  $3\sigma$  evidence for luminosity evolution (LE), a broken power-law LF with significant steepening at  $L \sim 10^{50}$  erg s<sup>-1</sup>, and an FR evolution that decreases monotonically with redshift (independent of LE and the thresholds). Thus, SGRBs may have been more luminous in the past with an FR delayed relative to the SFR as expected in the merger scenario.

*Unified Astronomy Thesaurus concepts:* [Gamma-ray bursts \(629\)](#)

## 1. Introduction

The bimodality of the distributions of the duration of the prompt emission of gamma-ray bursts (GRBs) that separates them into two classes, short and long (hereafter SGRBs and LGRBs), at the observer frame duration  $T_{90}^{\text{obs}} \sim 2$  s (Kouveliotou et al. 1993),<sup>8</sup> remains valid for rest-frame duration  $T_{90} = T_{90}^{\text{obs}}/Z$  after measurement of redshift  $Z = z + 1$ .<sup>9</sup> In addition, SGRBs tend to have harder spectra, and are located in the outskirts of older host galaxies rather than in star-forming galaxies with a younger stellar population (Frucheter et al. 2006; Wainwright et al. 2007). These differences have led to two separate progenitors: the collapse of massive stars (Woosley 1993; MacFadyen & Woosley 1999) for LGRBs and the merger of two neutron stars (NSs) or an NS and a black hole (BH) for SGRBs (Lattimer & Schramm 1976; Eichler et al. 1989; Narayan et al. 1992; Nakar 2007; Berger 2014; Nakar et al. 2006; Metzger & Berger 2012).

The possibility and eventual discovery of gravitational-wave (GW) radiation from several BH–BH mergers (Abbott et al. 2016a, 2016b, 2017a) and one NS–NS merger (GW170817; Abbott 2017b), which is associated with the SGRB 170817A, has made the determination of the intrinsic distributions, such as the luminosity function (LF),  $\Psi(L, Z)$ , luminosity evolution (LE),  $L(Z)$ , and formation rate (comoving density) evolution,

$\dot{\rho}(Z)$ , of SGRBs a critical issue (see, e.g., Wanderman & Prian 2015; Ghirlanda et al. 2016; Troja et al. 2017; Paul 2018; Zhang & Wang 2018; Petrillo et al. 2013; Beniamini & Piran 2019).

Categorizing GRBs into long and short classes is not straightforward, and some subclasses exist: for example, SGRBs followed by a low-flux long extended emission (hereafter SEE; Norris & Bonnell 2006). The nature of SEEs is still being debated (Dainotti et al. 2013, 2018; Kagawa et al. 2015), and there are arguments (Barkov & Pozanenko 2011) in favor of them having the same progenitors (merger events) as the usual SGRBs. Thus, we consider SGRBs and SEEs together in a combined sample. We aim to obtain a more robust determination of the above-mentioned intrinsic distributions using nonparametric (instead of commonly used forward fitting that involves several assumptions) methods, described in Section 2, and a selected sample of SGRBs with measured spectroscopic redshifts, described in Section 3. The results are presented in Section 4 followed by a summary and conclusion in Section 5.

## 2. The Methodology

Determination of the intrinsic distributions requires a sample with well-defined observational selection criteria, such a defined flux limit referred to as a *reliable sample*. The most readily available “reliable” samples are those with a well-defined detection threshold or energy flux limit,  $f > f_{\text{lim}}$ . For GRBs, one also requires redshift to obtain the luminosity and

<sup>8</sup>  $T_{90}$  is the time in which a burst emits from 5% to 95% of its total measured counts.

<sup>9</sup> The quantity  $Z = 1 + z$  is more convenient than  $z$  for describing the evolutionary functions at high redshifts. We refer to both variables as redshift.

its truncation:

$$L_i(Z) = 4\pi d_L^2(Z, \Omega) f_i K(Z, \alpha),$$

$$\text{for } f_i = f \text{ and } f_{\text{lim}}, \quad (1)$$

respectively. Here  $K(Z, \alpha)$  are the K-correction (Bloom 2001), where  $\alpha = d \ln f / d \ln \nu - 1$  is the photon number spectral index. We use energy fluxes, and hence luminosities, integrated over the Swift energy band 15–150 keV. To compute  $K$  we used a power law with exponential cutoff spectrum, that fits best to most GRBs, with the best-fit values taken from the online Third GRB Catalog (Lien et al. 2016). For nine cases for which the cutoff power law was not a possible fit we used the simple power law. The derived luminosities are shown in the right panel of Figure 2.<sup>10</sup> This information is used to determine the bivariate distribution  $\Psi(L, Z)$  taking into account the bias (the Malmquist bias) introduced by the flux limit. A common practice to account for this bias is to use a forward-fitting method (Butler et al. 2009), whereby a set of assumed *parametric functional forms* are fit to the data to determine the “best-fit values” of the many parameters of the functions, raising questions about the uniqueness of the results.

Nonparametric, nonbinning methods, such as the so-called  $V/V_{\text{max}}$  method and the  $C^-$  method of Lynden-Bell (1971), require no such assumptions and are more powerful, especially for small samples. However, as pointed out by Petrosian (1992), these methods require the critical assumption that the variables, in this case  $L$  and  $Z$ , are uncorrelated, which implies the physical assumption of no LE, i.e.,  $\Psi(L, Z) = \phi(L)\dot{\rho}(Z)$ . This shortcoming led to developments of the more powerful (also nonparametric, nonbinning) methods of Efron and Petrosian (1992), which does away with the no-LE assumption by testing whether  $L$  and  $Z$  are correlated. If correlated then it introduces a new variable  $L_0 \equiv L/g(Z)$  and finds the LE function,  $g(Z)$ , that yields an uncorrelated  $L_0$  and  $Z$ . For normalization of  $g(Z=1)=1$ ,  $L_0$  is the local  $z=0$  luminosity. Thus, the LF reads as

$$\Psi(L, Z) = \frac{\dot{\rho}(Z)}{g(Z)} \phi\left[\frac{L}{g(Z)}, \alpha_i\right], \quad (2)$$

where  $\alpha_i$  is the shape parameters.<sup>11</sup> One then can proceed with the determination of the local LF  $\psi(L_0)$  and density rate evolution  $\dot{\rho}(Z)$ . This combined Efron-Petrosian and Lynden-Bell (EP-L) method has been very useful for studies of evolution of GRBs (Petrosian et al. 2015). Thus, more papers dealing with GRB evolution use this method. Recent analyses of different LGRB samples (Lloyd et al. 1999; Lloyd & Petrosian 1999; Lloyd et al. 2000; Yonetoku et al. 2004; Dainotti et al. 2015; Petrosian et al. 2015; Yu et al. 2015; Pescalli et al. 2016; Tsvetkova et al. 2017; Lloyd-Ronning et al. 2019) show similar results, indicating that, contrary to the common assumptions, there is a significant LE, and that there is a considerable disagreement between LGRB formation rate (FR) and the star formation rate (SFR) at low redshifts ( $\dot{\rho}(z) > \text{SFR}$  for  $z < 1$ ). A similar high formation rate of

SGRBs at low redshifts will have profound consequences on the expected rate of GW sources. There have been several analyses of SGRBs (see, e.g., Guetta & Piran 2005; Wanderman & Prian 2015; Ghirlanda et al. 2016, Paul 2018; Yonetoku et al. 2004; Zhang & Wang 2018). The last two papers use the EP-L method and so-called pseudo-redshifts for samples of 45 and 239 sources, respectively, with somewhat different results.

We note, however, that many aspects of determination of a true LF, and its evolution continue to be debated. In particular, the unique aspect of the EP-L method, namely, the determination of correlation between luminosity and redshift (i.e., the LE) is sensitive to the flux threshold; using a lower threshold can lead to a stronger LE. Thus, in our past work on LGRBs and here we evaluate the evolution of the SGRB FR, the main focus of our paper, with and without the LE, which is a  $<3\sigma$  effect.

### 3. The Sample Selection

The Neil Gehrels Swift Observatory (Swift; Gehrels et al. 2004) allows the rapid follow-up (X-ray, optical/UV) observation after detection of the prompt emission. As of 2019 June, the Swift Burst Alert Telescope (BAT) instrument has observed 1309 GRBs (1190 LGRBs and 162 SGRBs and SEEs) with a given prompt flux limit. Of these, 472 have measured redshifts (339 LGRBs and 68 SGRBs and SEEs). The observational selection criteria of the samples with redshifts are not well defined because redshift measurements are complicated involving localization by X-ray Telescope (XRT) and optical/UV follow-up. Therefore, there is great difficulty in determining a well-defined flux limit, especially for samples with redshift. Swift has many triggering criteria for GRB detection in general (Howell et al. 2014). To account for this problem Lien et al. (2014) carry out extensive simulations to determine a detection efficiency function that can be used in the determination of the LF. However, these simulations are based on characteristics that are more appropriate for long GRBs. Carrying out similar simulations for SGRBs would be useful, but is beyond the scope of this Letter. To overcome this difficulty we have extensively searched in the *Swift* databases, and have identified a complete sample of 162 SGRBs and SEEs with known peak fluxes, referred to as the “parent sample.” This sample is defined as “complete” or “reliable” in the sense that we have all the information about the peak flux and the spectral features; it is the most comprehensive sample in the literature from 2005 December until 2019 June. From Norris & Bonnell (2006) we find a subsample of 68 SGRBs and SEEs with known redshifts (27 of which are SEE with redshift and are listed in Table 1). Figure 1 compares the differential flux distributions of the parent sample and the subsample with redshift.

As expected, the fraction of sources with redshifts decreases with decreasing flux, from 0.53 for  $f > f_c$  to 0.31 for  $f_c > f > f_{\text{min}}$ , with  $\log f_c = -6.3$  and  $\log f_{\text{min}} = -7.3$  (all fluxes hereafter will be in units of  $\text{erg cm}^{-2} \text{s}^{-1}$ ). We then use the Kolmogorov–Smirnov (KS) test to determine the probability,  $p$ , that subsamples with redshift are drawn from the parent sample, as a function of increasing flux limit starting with  $\log f_{\text{min}} = -7.3$ . As shown in the right panel of Figure 1 the  $p$ -value fluctuates between 0.6 and 0.9, eventually reaching a plateau with  $p \simeq 1$  for  $\log f > -6.34$ . To show the dependence of our results on the flux limit, we analyzed three samples: one with flux limit  $\log f_{\text{lim}} = -6.25$  well above the fluctuating part related to the probability that the samples are drawn by the same parent

<sup>10</sup> Here  $d_L$  is the luminosity distance using the Hubble constant  $H_0 = 0.70 \text{ km}^{-1} \text{ s}^{-1} \text{ Mpc}^{-1}$ , and density parameters  $\Omega_m = 0.3$  and  $\Omega_\Lambda = 0.7$ .

<sup>11</sup> For a small sample of sources determination of the evolution of the shape parameters is difficult to obtain. Here we assume that they are independent of the redshift.

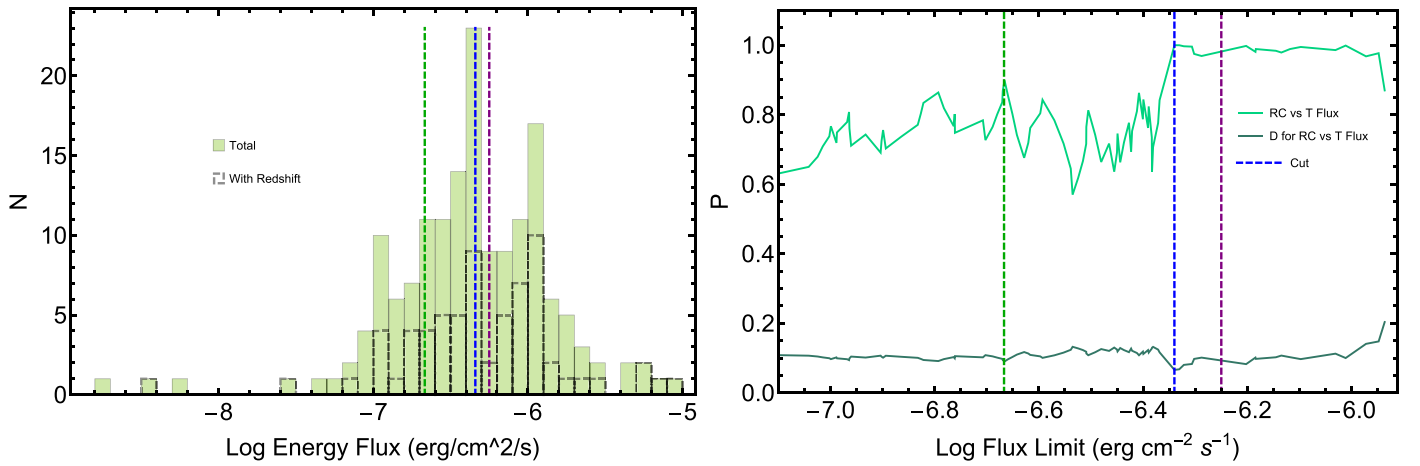


**Figure 1.** Left panel: histogram of the differential distribution of the fluxes of the 162 SGRBs and SEEs (green filled bars), the “parent sample,” and the 68 with redshift (dashed black bars). Right panel: the probability ( $p$ -value) as a function of the flux limit that subsamples with redshift are drawn from the parent sample obtained by KS test (upper bright green curve). The lower darker green line shows the maximum distance between the two cumulative distribution used in the KS test to obtain the  $p$ -values (see examples in Figure 2). The vertical dashed green, blue, and purple lines, in both panels, show the flux limits of  $\log f_{\text{lim}} = -6.67$ ,  $\log f_{\text{lim}} = -6.34$ , and  $\log f_{\text{lim}} = -6.25$  (in units of  $\text{erg cm}^{-2} \text{s}^{-1}$ ) with  $p$ -values of 0.9, 1, and 1, respectively.

**Table 1**  
SEE GRBs with Known Redshift

Gamma-Ray Burst	Alpha	Epeak (keV)	Energy Flux 15-150 keV ( $\text{erg cm}^{-2} \text{s}^{-1}$ )	T90 (s)	SEE Source	$z$	$z$ Source
050724A	-0.78	77.81430	9.53E-07	96	REF[7,9,10]	0.2570	G/REF[16]
050911	-0.95	pl	2.69E-07	16.2	REF[7,8,15]	1.1650	REF[3]
051016B	2.71	44.03600	1.17E-07	4	REF[9,11,14]	0.9364	G/REF[16]
051227	-1.03	pl	1.96E-07	114.6	REF[5,6,11]	0.7140	G
060306	-0.91	140.58500	4.67E-07	61.2	REF[4,7]	1.5590	G
060607A	0.39	227.35400	3.22E-07	102.2	REF[7]	3.0749	G/REF[16]
060614	-1.03	230.29500	7.62E-07	108.7	REF[5,7,8]	0.1250	G/REF[16]
060814	-0.46	152.90200	9.31E-07	145.3	REF[7]	0.8400	REF[16]
060912A	-1.82	590.16700	6.55E-07	5	REF[1]	0.9370	G/REF[16]
061006	0.04	305.73800	1.85E-06	129.9	REF[5,7,9]	0.4400	G
061021	-0.89	461.80200	8.20E-07	46.2	REF[4,8]	0.3463	G
061210	0.03	256.95100	7.26E-06	85.3	REF[7,8,9]	0.4095	G/REF[16]
070223	-1.03	pl	2.23E-07	88.5	REF[7]	1.6295	G
070506	-1.19	pl	6.84E-08	4.3	REF[9,14]	2.3100	REF[16]
070714B	-0.70	9794.42000	1.05E-06	64	REF[7,8,11]	0.9200	G/REF[16]
080603B	-1.08	pl	1.26E-07	60	REF[7]	2.6900	G/REF[16]
080913	0.07	67.87210	2.16E-07	8	REF[2,3]	6.4400	G/REF[16]
090530	0.71	64.77000	4.08E-07	48	REF[7,14]	1.2660	G/REF[16]
090927	-0.94	851.06400	4.57E-07	2.2	REF[9,14]	1.3700	REF[16]
100704A	-0.77	pl	6.28E-07	197.5	REF[7]	3.6000	REF[16]
100814A	0.34	171.65700	4.99E-07	174.5	REF[7]	1.4400	G/REF[16]
100816A	0.70	108.27700	1.00E-07	2.9	REF[7,14,15]	0.8040	G/REF[16]
100906A	0.90	78.45730	1.07E-06	114.4	REF[7]	1.7270	G/REF[16]
111005A	-1.42	pl	3.98E-07	26	REF[13]	0.0133	G
111228A	-1.38	214.95800	1.16E-06	101.2	REF[9]	0.7140	G/REF[16]
150424A	-0.11	998.74700	5.70E-06	91	REF[11,12,15]	0.3000	REF[16]
160410A	0.77	197.81600	1.15E-06	8.2	REF[11,14,15]	1.7200	G/REF[16]

**Notes.** Epeak assumes cutoff power law unless otherwise noted.

REF[1] = Levan et al. (2007), REF[2] = Ghirlanda et al. (2009), REF[3] = Zhang et al. (2009), REF[4] = Minaev et al. (2010), REF[5] = Norris et al. (2010), REF[6] = Gompertz et al. (2013), REF[7] = Hu et al. (2014), REF[8] = van Putten et al. (2014), REF[9] = Kaneko et al. (2015), REF[10] = Abbott et al. (2017c), REF[11] = Gibson et al. (2017), REF[12] = Knust et al. (2017), REF[13] = Wang et al. (2017), REF[14] = Anand et al. (2018), REF[15] = Kagawa et al. (2019), REF[16] = [https://swift.gsfc.nasa.gov/archive/grb\\_table/](https://swift.gsfc.nasa.gov/archive/grb_table/), G = <http://www.mpe.mpg.de/~jcg/grbgen.html>.

distribution (see the left panel of Figure 1, purple line) and one with  $\log f_{\text{lim}} = -6.34$  at the start of the plateau (both with  $p = 1$ ), and a third larger sample with  $\log f_{\text{lim}} = -6.67$ , where there is a peak (with  $p = 0.9$ ). (The three limits are shown by the vertical

dashed purple, blue, and green lines in Figure 1). The first two samples show very similar results (see Figures 2 and 3). Thus, in what follows we present results on the LF and FR for the larger sample with  $\log f_{\text{lim}} = -6.34$  (our “Sample 1”) consisting of 32

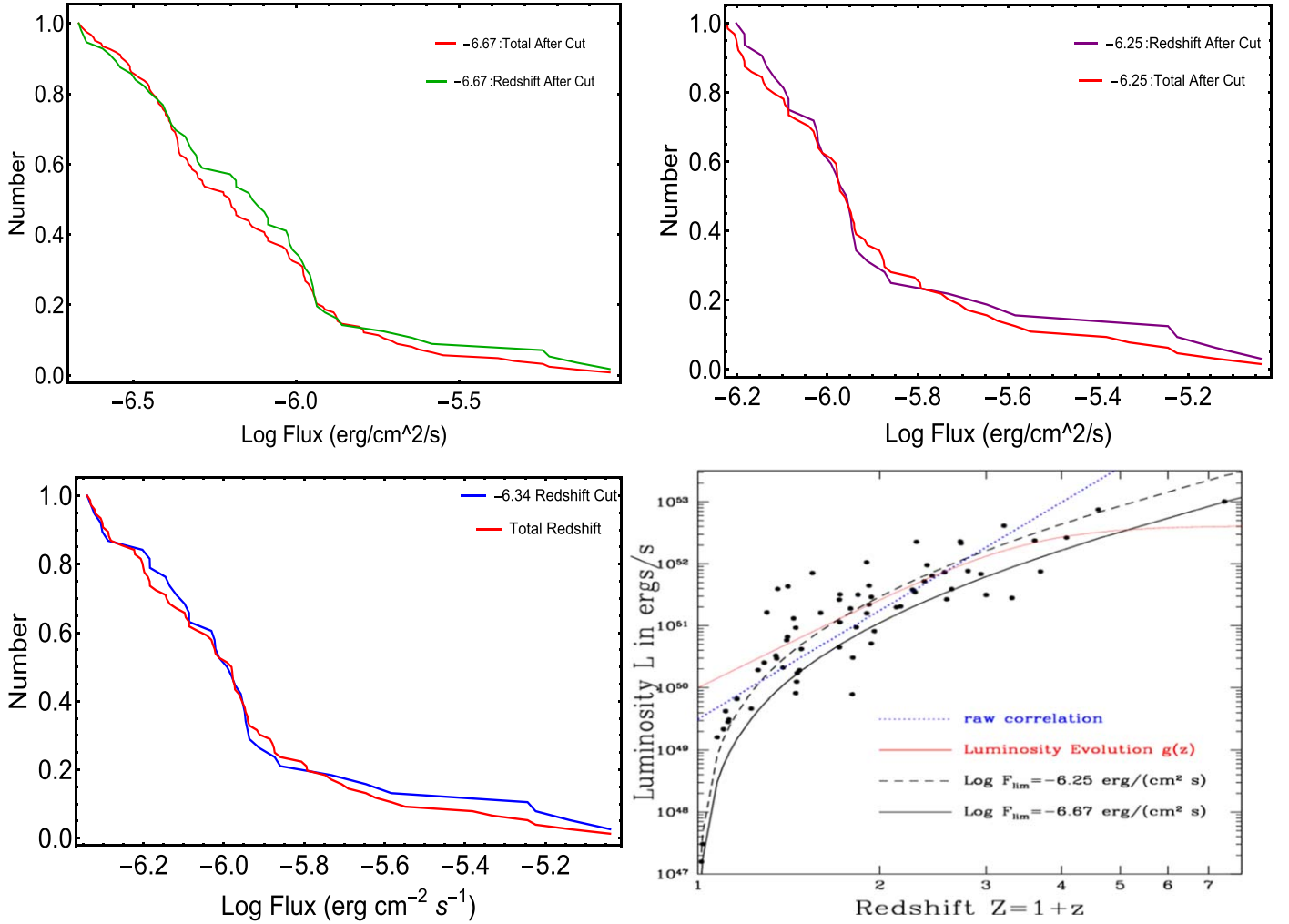


**Figure 2.** Normalized cumulative distribution of the parent (red lines) and subsamples with redshift (green, purple, and blue lines) used in the KS test for the three samples with  $\log f_{\text{lim}} = -6.67$  (top left),  $-6.34$  (bottom left), and  $-6.25$  (top right). Bottom right panel shows the luminosity vs. redshift distribution of all SGRBs and SEEs with known redshifts. The blue dotted line shows the raw correlation between luminosity and redshift, part of which is due to the truncation of the data caused by observational selection effects. The dashed and solid black lines show the truncation boundaries,  $L_{\text{min}}(z)$ , obtained for the cuts at  $\log F_{\text{lim}} = -6.34$  and  $-6.67$   $\text{erg cm}^{-2}\text{s}^{-1}$ , respectively. The red curve shows the intrinsic correlation obtained using the procedures described in Section 3.

SGRBs with redshift, and for “Sample 2” with  $\log f_{\text{lim}} = -6.67$ , consisting of 56 sources with known redshifts (34 SGRBs and 22 SEE GRBs). The normalized cumulative distributions of fluxes of the three parent samples and their respective subsamples with  $z$ , used in the KS test, are shown on Figure 2. The bottom right panel of Figure 2 shows the luminosity versus redshift of all sources and the two curves (the dashed and solid lines show the luminosity truncation,  $L_{\text{min}}(z)$ , obtained from Equation (1), for  $\log f_{\text{lim}} = -6.34$  and  $\log f_{\text{lim}} = -6.67$ , respectively).

## 4. Results

We determine the shape and evolution of the LF  $\Psi(L, Z)$  in Equation (2), using the observed  $L - Z$  diagram corrected for biases introduced by the truncation in the samples, shown in the right panel of Figure 2.

### 4.1. Luminosity Evolution

As indicated in the right panel of Figure 2 (blue line), the luminosity and redshift are highly correlated, but part of this correlation is due to truncation shown by the limiting curves. We use the Efron & Petrosian (1992) method to correct for this

bias with a modified Kendall’s  $\tau$  statistics. We find a value  $\tau < 3$  indicating a  $\sim 3\sigma$  evidence for an intrinsic correlation or LE for all three samples. We adopt a commonly used single parameter evolutionary function  $Z^k$  with slight modification:

$$g_k(Z) = \frac{Z^k}{1 + (Z/Z_c)^k}. \quad (3)$$

The denominator has been added to reduce the rate of evolution at high redshifts (here chosen as  $Z_c = 3.5$ ) where the cosmic expansion timescale is reduced considerably from its current ( $Z \leq 2$ ) value. This function has been proven very useful for studies of high-redshift AGNs and GRBs (Singal et al. 2011; Petrosian et al. 2015; Dainotti et al. 2013, 2015, 2017). As demonstrated in Dainotti et al. (2015) the difference between the results based on the simple function  $g_k(Z) = Z^k$  and those based on Equation (3) is  $< 2\sigma$ . The variation of  $\tau$  with  $k$  is shown in Figure 3, giving the best value of  $k$  (when  $\tau = 0$ ) and its  $1\sigma$  range of uncertainty (given by  $|\tau| \leq 1$ ) of  $k = 5.4_{-0.5}^{+0.93}$ ,  $5.0_{-1.7}^{+1.0}$  and  $4.8_{-0.5}^{+0.5}$  for  $\log f_{\text{lim}} = -6.25$ ,  $-6.34$ , and  $-6.67$ , respectively. Thus, regardless of the flux limit the

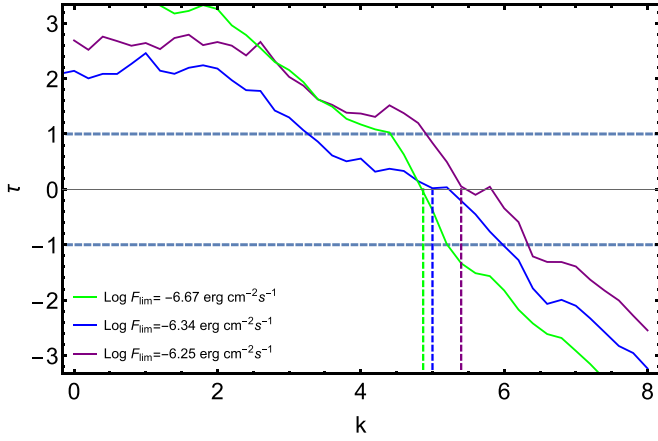


**Figure 3.** Test statistic  $\tau$  vs. luminosity evolution index  $k$ , defined in Equation (3) with vertical lines giving the best values of  $k$  that yields a local luminosity  $L_0 = L/g_k(Z)$  independent of (or uncorrelated with) redshift for the three samples with log flux limits of  $-6.25$  (brown),  $-6.34$  (blue), and  $-6.67$  (green). The vertical dotted lines showing the best (and  $1\sigma$ ) values of  $k = 5.4^{+0.93}_{-0.5}$ ,  $5.0^{+1.0}_{-1.7}$ , and  $4.8^{+0.5}_{-0.5}$ , respectively.

three values of  $k$  appear to be strong (but  $< 3\sigma$ ) evidence of LE with  $g_k(Z) \propto Z^{-5}$  for  $Z \leq 3$ .

Similar, but slightly slower LE was found for long GRBs (see, e.g., Petrosian et al. 2015). However, if one underestimates  $f_{\text{lim}}$ , one would obtain stronger evolution eventually reaching the maximum obtained from the raw data ignoring the effects of the truncation (i.e.,  $f_{\text{lim}} \rightarrow 0$ ). Recently, Bryant et al. (2020) demonstrated this effect with simulations based on LGRB characteristics. However, the three samples with different flux limits show very similar results, thus proving that this objection does not apply here. This effect comes into play when the truncation curve falls below most of the points, which, as evident in the bottom right panel of Figure 2, is not the case here. On the other hand, if SGRB progenitors are merging compact stars, it is not clear why such well-defined events would depend strongly on cosmological epoch of their occurrence. However, since we have meager observations on the generation of the electromagnetic radiation of the so-called kilonovae produced during such mergers, the existence of an LE cannot be ruled out. Nevertheless, because (i) the evidence is less than  $3\sigma$ , (ii) there are uncertainties about the flux threshold, and (iii) there may be theoretical arguments against it, we evaluate the FRE of the SGRBs, our main focus here, with and without inclusion of the LE.

#### 4.2. Luminosity Function and Rate Evolution

Having established the independence of luminosity  $L_0$  and  $Z$  we can then proceed to obtain their distribution following the steps of the EP-L method. This method gives nonparametric histograms of the cumulative distributions

$$\begin{aligned} \Phi(L_0) &= \int_{L_0}^{\infty} \phi(L'_0) dL'_0 \text{ and } \sigma(Z) \\ &= \int_1^Z \dot{\rho}(Z') \left( \frac{dV}{dz'} \right) \frac{dz'}{Z'}, \end{aligned} \quad (4)$$

derivatives of which give the differential distributions. Here  $V(Z)$  is the comoving volume up to  $Z$ . Top and bottom left and middle panels of Figure 4 show the two cumulative distributions we obtain with the EP-L method, compared to raw cumulative counts (not corrected for the truncation), for the two

samples ( $\log f_{\text{lim}} = -6.67$ , upper and  $-6.34$ , lower), respectively. In the case of the rate evolution, shown in the middle panels, we show the corrected values including LE ( $k = 5.0$ , red) and without LE ( $k = 0$ , blue). It is evident the two samples give very similar results. Thus, very similar results will be given also for the sample at  $\log f_{\text{lim}} = -6.25$ , not shown to avoid cluttering the pictures. Nonparametric derivatives of these histograms can be obtained directly from the data as well. However, given that the cumulative distributions are somewhat noisy, we fit the cumulative distributions with analytic forms (broken power laws). The forms and the values of the parameters are shown inside the panels of Figure 4. For the LF the two samples are fit by exactly the same functions, but for cumulative rate evolution the results are slightly different as a comparison with fitted parameter values on the top and bottom panels would indicate.

The differential LF,  $\psi(L_0) = -d\Phi(L_0)/dL_0$ , obtained from the fitted forms (identical for both samples) is shown in the top right panel of Figure 4, and the differential density rate evolution,  $\dot{\rho}(z) = Z[d\sigma(z)/dz]/[dV(z)/dz]$ , for both samples, with and without LE, is shown in the bottom right panel of this figure showing some range of possibilities and thus uncertainties between the two samples, with and without accounting for LE. We have also plotted curves for delayed SFR with a power-law delay distribution with three indexes taken from Paul (2018) normalized at their peak values. We can see from the bottom right panel of Figure 4 that there is agreement with Paul (2018) for ranges of redshift between  $z = 0.10$  and  $z \sim 1$ .

## 5. Summary and Discussion

From a total sample of 162 GRBs (118 SGRBs and 44 SEE GRBs) with known redshifts and spectra we have selected three subsamples with flux limits of  $\log f_{\text{lim}} = -6.25$ ,  $6.34$ , and  $-6.67$  consisting of 32 and 34 SGRBs and 56 GRBs (34 SGRBs and 22 SEE GRBs). These samples according to the KS tests have probabilities of 1, 1, and 0.9, respectively, that are drawn from the “parent samples” consisting of all sources (with or without redshift) with the same flux limits. Using the nonparametric combined EP-L method we obtain the following results, which are very similar and compatible with  $1\sigma$  for the three samples.

1. For the three samples we find very similar evidence of a  $\leq 3\sigma$  LE,  $L(Z) \propto Z^{-5}$  at low  $z$  tending to constant value at  $z > 2.5$ , that is much stronger than  $Z^{-3}$  obtained for LGRBs.
2. After correction for the LE, we derive the cumulative LF, and its derivative the differential LF, which unlike those of LGRBs, that can be fit with a simple broken power law, shows steepening at (local) luminosities  $L_0 < 10^{50} \text{ erg s}^{-1}$  with an index equal to that at high luminosities of  $L > 10^{51.6} \text{ erg s}^{-1}$ , possibly caused by an excess of low-redshift sources. Most forward-fitting (FF) methods (see, e.g., Wanderman & Prian 2015) assume a priori a simple broken power law form for the LF of SGRBs. Our results, obtained directly from the data nonparametrically and without any assumptions, indicates that, unlike LGRBs, a power law with one break may not provide an adequate description of the LF of SGRBs.
3. With the same procedure we find the cumulative and the differential comoving density rate evolution with redshift.

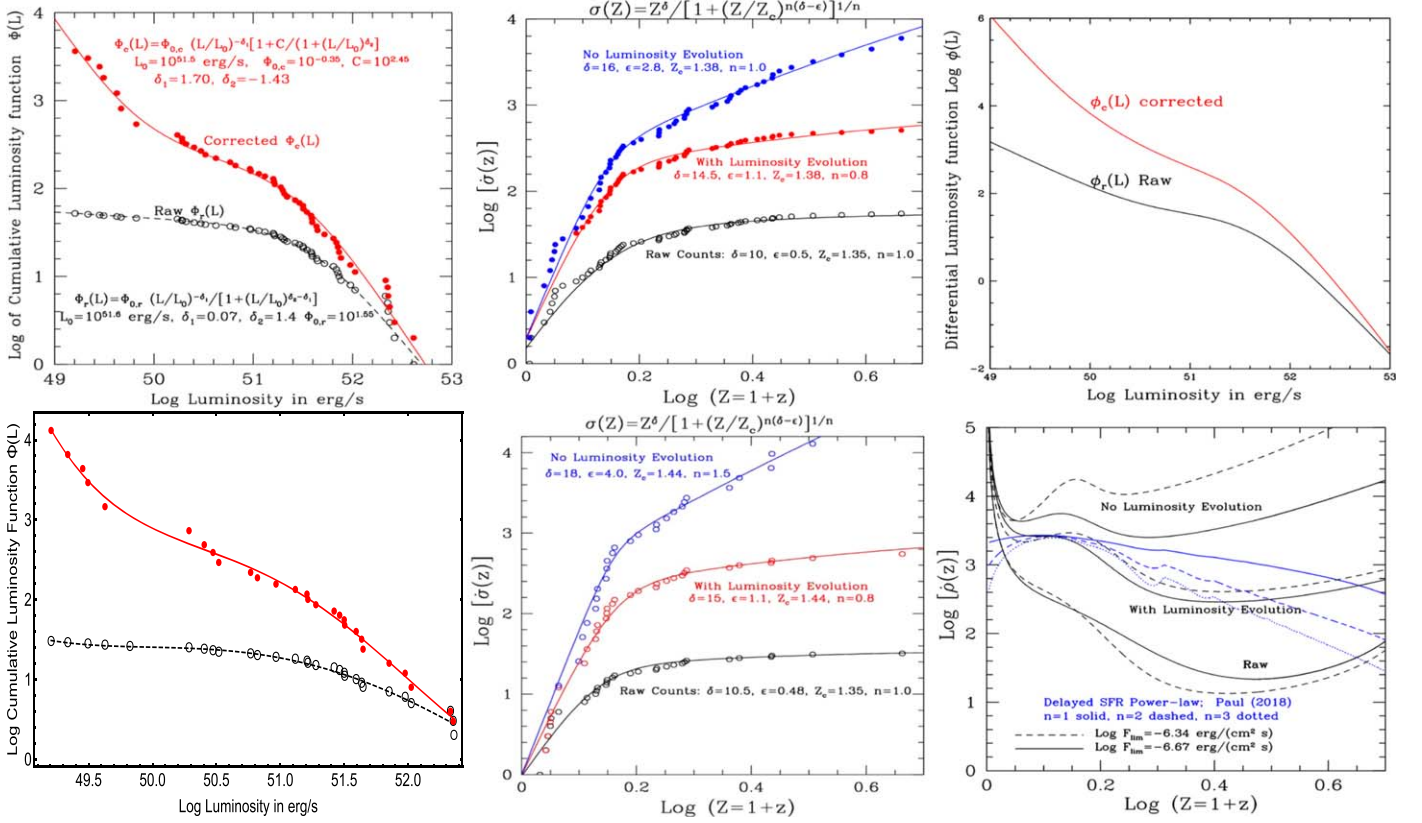


**Figure 4.** The cumulative LF,  $\Phi(L_0)$ , is shown in the left panel. In the left panel raw data are shown with black points, while with red with the EP-L method, but with no luminosity evolution. The density RE,  $\dot{\sigma}(Z)$ , is shown in middle panel for Sample 2 (top panel,  $\log F_{\text{lim}} = -6.67$ ), and Sample 1 (bottom panel,  $\log F_{\text{lim}} = -6.34$ ). In the middle panel the black points show the raw counts  $N(>L_0)$  and  $N(<Z)$  (uncorrected for truncation). The red points are obtained by the EP-L nonparametric method correcting for truncation and LE. The blue points in the middle panels ignore LE (i.e., set  $k=0$ ). The lines on the left represent (identical) power-law fits with two breaks, with their forms and parameters given inside the top panel. There are slight differences between the values of the parameters for the two samples. The analytic functions are used to obtain the differential distributions  $\psi(L_0) = -d\Phi(L_0)/dL_0$  shown in the top right panel (same for both samples), and  $\dot{\rho}(Z) = Z(d\dot{\sigma}(Z)/dZ)/(dV/dZ)$  shown in the bottom panel for Samples 1 (dashed) and 2 (solid) (raw, with LE, and without LE). The  $\dot{\sigma}$  curve for the no-LE case is steeper in the bottom middle panel giving rise to higher density rate evolution,  $\dot{\rho}(z)$ , shown by the dashed lines in bottom right panel. In this panel, we also show three curves (long-dashed, dashed, and dotted) taken from the Paul (2018) calculation of the delayed SFR with a power-law distribution of the delay times with indexes 1, 2, and 3, respectively.

Here, we obtain the rate evolution with and without inclusion of the  $< 3\sigma$  LE. In general, these rate decrease rapidly at low  $z$ , but flatten out at higher  $z$ . Inclusion of the LE yields a monotonically decreasing rate up to  $z=2.5$ . Beyond this, the rate increases slowly but this behavior is highly uncertain because of the small number of sources with  $z > 3$ . At very low redshifts this rate is in disagreement with the SFR (which increases rapidly as  $Z^{2.7}$  up to  $Z \sim 3$ ). This low-redshift behavior is similar to that found for LGRBs. But unlike LGRBs, the SGRB rate disagrees with the standard SFR at high redshifts too. It should be noted that there are very few SGRBs at  $z < 0.1$  and  $z > 3$  making these portions of the rate more uncertain. On the other hand, the somewhat monotonic decrease, especially with LE, is what is expected for events, such as merging compact binaries, with considerable time delay relative to SFR (see, e.g., Wanderman & Prián 2015 and Paul 2018), as shown in Figure 4 (bottom right), such expected rates agree with our results in the mid-redshift range.

These results on cosmological distributions and evolution of SGRBs are based on a well-defined and relatively sizable “reliable sample” with measured redshifts using powerful

nonparametric and nonbinning methods. In the future we will repeat the same treatment to further constrain the density rate evolution and the luminosity function by increasing the sample size. This will be possible by inclusion of GRBs observed by other instruments such as Konus-Wind and Fermi-GBM. The nonparametric methods used here are ideally suited for combining data from different instruments with different energy bands and selection criteria. With more data and more accurate determination of the FR of SGRBs it may be possible to constrain the parameters of the delayed SFR models.

M.G.D. acknowledges the support of the American Astronomical Society Chretienne Fellowship and Miniatura2 grant from the Polish Ministry of Science and Education that allowed her to be hosted at Stanford in 2018–2019. L.B. acknowledges the support by the U.S. Department of Energy, Office of Science, Office of Workforce Development for Teachers and Scientists (WDTS) under the Science Undergraduate Laboratory Internships Program (SULI). M.G.D. acknowledges the support of the American Astronomical Society Chretienne Fellowship that allow her to be hosted at Stanford in 2018–2019 and NAOJ Division of Science for the current support. M.G.D. is grateful to Dr. Cuellar for managing the SULI program. We are grateful to Hannah Yasin Hashai for

useful discussion about our results. M.G.D. acknowledges the support of Miniatura2 from the Polish Ministry of Society.

### ORCID iDs

M. G. Dainotti  <https://orcid.org/0000-0003-4442-8546>

V. Petrosian  <https://orcid.org/0000-0002-2670-8942>

### References

- Abbott, B. P. 2017b, in Centennial of General Relativity: A Celebration, ed. C. A. Z. Vasconcellos (Singapore: World Scientific Publishing Co. Pte. Ltd.), 291
- Abbott, B. P., Abbott, R., Abbott, T. D., et al. 2016, *ApJL*, 832, L21
- Abbott, B. P., Abbott, R., Abbott, T. D., et al. 2016b, *PhRvL*, 116, 241102
- Abbott, B. P., Abbott, R., Abbott, T. D., et al. 2017a, *PhRvL*, 96, 122006
- Abbott, B. P., Abbott, R., Abbott, T. D., et al. 2017c, *ApJL*, 848, L13
- Anand, N., Shahid, M., & Resmi, L. 2018, *MNRAS*, 481, 4332
- Barkov, M. V., & Pozanenko, A. S. 2011, *MNRAS*, 417, 2161
- Beniamini, P., & Piran, T. 2019, *MNRAS*, 487, 4847
- Berger, E. 2014, *A&A*, 52, 43
- Bloom, J. S., Frail, D. A., & Sari, R. 2001, *AJ*, 121, 2879
- Bryant, C., Osborne, J. A., & Shahmoradi, A. 2020, arXiv:2010.02935v1
- Butler, N. R., Kocevski, D., & Bloom, J. S. 2009, *ApJ*, 694, 76
- Dainotti, M., Del Vecchio, R., & Tarnopolski, M. 2018, *AdAst*, 2018, 969503
- Dainotti, M., Petrosian, V., Willingale, R., et al. 2015, *MNRAS*, 451, 3898
- Dainotti, M. G., Hernandez, X., Postnikov, S., et al. 2017, *ApJ*, 848, 88
- Dainotti, M. G., Petrosian, V., Singal, J., & Ostrowski, M. 2013, *ApJ*, 774, 157
- Efron, B., & Petrosian, V. 1992, *ApJ*, 399, 345
- Eichler, D., Livio, M., Piran, T., & Schramm, D. 1989, *Natur*, 340, 126
- Frucheter, A. S., Levan, A. J., Strolger, L., et al. 2006, *Natur*, 441, 463
- Gehrels, N., Chincarini, G., Giommi, P., et al. 2004, *ApJ*, 611, 1005
- Ghirlanda, G., Nava, L., Ghisellini, G., Celotti, A., & Firmani, C. 2009, *A&A*, 496, 585
- Ghirlanda, G., Salafia, O. S., Pescalli, A., et al. 2016, *A&A*, 594, A84
- Gibson, S. L., Wynn, G. A., Gompertz, B. P., & O'Brien, P. T. 2017, *MNRAS*, 470, 4925
- Gompertz, B. P., O'Brien, P. T., Wynn, G. A., & Rowlinson, A. 2013, *MNRAS*, 431, 1745
- Guetta, D., & Piran, T. 2005, *A&A*, 435, 421G
- Howell, E. J., Coward, D. M., Stratta, G., Gendre, B., & Zhou, H. 2014, *MNRAS*, 444, 15
- Hu, Y.-D., Liang, E.-W., Xi, S.-Q., et al. 2014, *ApJ*, 789, 145
- Kagawa, Y., Yonetoku, D., Sawano, T., et al. 2019, *ApJ*, 877, 147
- Kagawa, Y., Yonetoku, D., Sawano, Tg., et al. 2015, *ApJ*, 811, 4
- Kaneko, Y., Bostanci, Z. F., Göğüş, E., & Lin, L. 2015, *MNRAS*, 452, 824
- Knust, F., Greiner, J., van Eerten, H. J., et al. 2017, *A&A*, 607, A84
- Kouveliotou, C., Meegan, C. A., Fishman, G. J., et al. 1993, *ApJL*, 413, L101
- Lattimer, J. M., & Schramm, D. N. 1976, *ApJ*, 210, 549
- Levan, A. J., Jakobsson, P., Hurkett, C., et al. 2007, *MNRAS*, 378, 1439
- Lien, A., Alexandrova, O., & Zaslavsky, A. 2016, *ApJ*, 829, 47
- Lien, A., Sakamoto, T., Gehrels, N., et al. 2014, *ApJL*, 783, 24L
- Lloyd, D. A., Hernquist, L., & Heyl, J. S. 1999, in ASP Conf. Ser. 271, Neutron Stars in Supernova Remnants, ed. P. O. Slane & B. M. Gaensler (San Francisco, CA: ASP), 323
- Lloyd, N. M., & Petrosian, V. 1999, *ApJ*, 511, 550
- Lloyd, N. M., Petrosian, V., & Mallozzi, R. S. 2000, *ApJ*, 534, 227
- Lloyd-Ronning, N. M., Aykutalp, A., & Johnson, J. L. 2019, *MNRAS*, 488, 5823
- MacFadyen, A. I., & Woosley, S. E. 1999, *ApJ*, 524, 262
- Metzger, B. D., & Berger, E. 2012, *ApJ*, 746, 48
- Minaev, P. Yu., Pozanenko, A. S., & Loznikov, V. M. 2010, *AstL*, 36, 707
- Nakar, E. 2007, *AdSpr*, 40, 1224
- Nakar, E., Gal-Yam, A., & Fox, D. B. 2006, *ApJ*, 650, 281
- Narayan, R., Paczynski, B., & Piran, T. 1992, *ApJL*, 395, L83
- Norris, J. P., & Bonnell, J. T. 2006, *ApJ*, 643, 266
- Norris, J. P., Gehrels, N., & Scargle, J. D. 2010, *ApJ*, 717, 411
- Paul, D. 2018, *MNRAS*, 477, 4275
- Pescalli, A., Ghirlanda, G., Salvaterra, r., et al. 2016, *A&A*, 587, A40
- Petrillo, C. E., Dietz, A., & Cavaglia, M. 2013, *ApJ*, 767, 140
- Petrosian, V. 1992, *BAAS*, 24, 756
- Petrosian, V., Kitanidis, E., & Kocevski, D. 2015, *ApJ*, 806, 44
- Singal, J., Petrosian, V., Lawrence, A., & Stawarz, L. 2011, *ApJ*, 743, 104
- Troja, E., Lipunov, V. M., Mundell, C. G., et al. 2017, *Natur*, 547, 425
- Tsvetkova, A., Frederiks, D., Golenetskii, S., et al. 2017, *ApJ*, 850, 161
- van Putten, M. H. P. M., Lee, G. M., Della Valle, M., Amati, L., & Levinson, A. 2014, *MNRAS*, 444, L58
- Wainwright, C., Berger, E., & Penprase, B. E. 2007, *ApJ*, 657, 367
- Wanderman, D., & Prian, T. 2015, *MNRAS*, 448, 3026
- Wang, Y.-Z., Huang, Y.-J., Liang, Y.-F., et al. 2017, *ApJL*, 851, L20
- Woosley, S. E. 1993, *ApJ*, 405, 273
- Xu, M., & Huang, Y. F. 2012, *A&A*, 538, 134
- Yonetoku, D., Murakami, T., Nakamura, T., et al. 2004, *ApJ*, 609, 953
- Yu, H., Wang, F. Y., Dai, Z. G., & Cheng, K. S. 2015, *ApJS*, 218, 13
- Zhang, B., Zhang, B.-B., Virgili, F. J., et al. 2009, *ApJ*, 703, 1696
- Zhang, G. Q., & Wang, F. Y. 2018, *ApJ*, 852, 1